

Visual Odometry with Transformers

Vladimir Yugay*

Duy-Kien Nguyen*

Theo Gevers

Cees G. M. Snoek

Martin R. Oswald

University of Amsterdam

vladimiryugay.github.io/vot

Abstract

Despite the rapid development of large 3D models, classical optimization-based approaches dominate the field of visual odometry (VO). Thus, current approaches to VO heavily rely on camera parameters and many hand-crafted components, most of which involve complex bundle adjustment and feature matching processes. Although disregarded in the literature, we find it problematic in terms of both (1) speed, that performs bundle adjustment requires a significant amount of time; and (2) scalability, as hand-crafted components struggle to learn from large-scale training data. In this work, we introduce a simple yet efficient architecture, **Visual odometry Transformer (VoT)**, that formulates monocular visual odometry as a direct relative pose regression problem. Our approach streamlines the monocular visual odometry pipeline in an end-to-end manner, effectively eliminating the need for handcrafted components such as bundle adjustment, feature matching, or camera calibration. We show that VoT is up to ~ 4 times faster than traditional approaches, yet with competitive or better performance. Compared to recent 3D foundation models, VoT runs ~ 10 times faster with strong scaling behavior in terms of both model sizes and training data. Moreover, VoT generalizes well in both low-data regimes and previously unseen scenarios, reducing the gap between optimization-based and end-to-end approaches. Code will be released.

1. Introduction

The goal of monocular visual odometry is to estimate a camera's position and orientation from a sequence of video frames [5]. In recent years, monocular visual odometry has gained increasing attention across various fields, including augmented reality, virtual reality, autonomous driv-

*Equal contribution. Corresponding authors: {VovikTYL, kienduynguyen94}@gmail.com

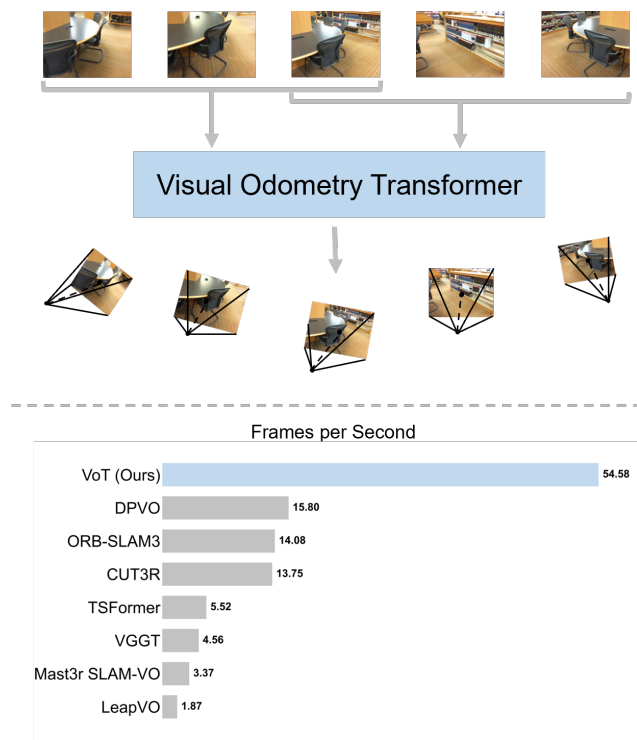


Figure 1. **Visual Odometry Transformer**. The metric camera trajectory (top) is derived by passing intersecting windows of images through a feed-forward model that estimates relative camera poses between them, subsequently integrating these poses into a unified trajectory. VoT does not rely on camera parameters or test-time optimization. Moreover, our method is more than $3\times$ faster than all the baselines.

ing, and robotics. This growing interest is particularly notable when compared to systems that rely on stereo vision [12, 37] or multimodal inputs, such as visual-inertial

odometry [14, 33]. Although monocular setups present greater challenges, their simplicity in deployment enables even broader applicability in real-world scenarios. Therefore, this paper focuses on monocular visual odometry using neural network-based approaches.

There has been rapid progress in monocular visual odometry over a short period, highlighting the potential of learning-based approaches. The dominant approach brought by this progress utilizes learnable features as well as differentiable optimization layers within deep learning frameworks [8, 30]. While these designs improve convergence and robustness in real-world conditions, their performance critically relies on post-processing techniques, such as bundle adjustment or feature matching, to refine the estimates of camera poses. However, the limitations are still evident in real-world applications as the prediction in the wild has to undergo a slow post-processing process. Furthermore, hand-crafted elements incorporate prior domain knowledge, making it hard to scale with training data.

To this end, we shift our attention to the fast and scalable architecture. Recent successes in machine translation [32], image recognition [11], and object detection [7] demonstrated that a simple transformer is effective enough for end-to-end structured prediction. By learning a mapping directly from video input to camera poses, the model becomes less dependent on predefined priors and can better capture complex temporal and spatial relationships. This design choice aligns with recent evidence [22], suggesting that reducing inductive bias enables models to generalize more effectively from data. Most importantly, the end-to-end formulation enables direct prediction of camera trajectories without relying on heavy post-processing.

In this paper, we introduce the **Visual odometry Transformer (VoT)**, a fully end-to-end framework for monocular visual odometry. Our approach formulates visual odometry as a direct pose prediction task. It mainly differs from previous models in the use of encoder-decoder architecture. The encoder is initialized with a pre-trained backbone to extract image features, while the decoder employs both temporal and spatial attention to model interactions across frames. The decouple between feature extraction with encoder and feature interaction with decoder significantly boosts the inference speed and scalability of the model. Fig. 1 shows that our end-to-end model is around ten times faster than 3D foundation models and at least three times than those with hand-crafted components while exhibiting similar or even better performance on multiple benchmarks.

Our key contributions can be summarized as follows:

- VoT is the *simple* architecture by far for visual odometry as it commissions the pre-trained transformer as encoder and a light-weight transformer as decoder. This design inherently leads to significant speedup in our runtime while

still being scalable in terms of both model sizes and training data;

- For the first time, we achieve competent performance on several benchmarks of visual odometry without using any hand-crafted components and simply predicting camera poses in an end-to-end manner;
- We showcase that end-to-end learning with VoT is beneficial especially when large-scale train data is available while it still generalizes well to low-regime data and unseen scenarios.

2. Related Work

Visual odometry. Visual odometry systems estimate the position and orientation of a camera using video input. Unlike SLAM, which corrects errors via loop closure [5, 6, 43], these systems have to cope with camera tracking errors (drift). Many different modalities of visual odometry have been explored by past work, including visual-inertial odometry [14, 33] and stereo visual odometry [12, 37]. While improving the overall performance, the multi-modal setting limits the potential to scale up the system with training data. Here, we focus on the monocular case, where the only input is a monocular video stream. Traditional monocular visual odometry methods [6, 12, 13] are sensitive to illumination and rolling shutter artifacts, and more importantly, cannot adequately estimate the scale of the scene. To overcome these limitations, VoT leverages a large pre-trained encoder and extensive training data for robust generalization.

Deep monocular visual odometry. Deep learning has further advanced monocular visual odometry in both supervised [28, 30, 38, 40] and unsupervised [19, 25, 26, 42] settings. DeepVO [38] uses recurrent networks for temporal modeling, while SfMLearner [26] jointly learns depth and motion without labels. DPVO [30], inspired by RAFT [29], combines flow, confidence, and geometry with iterative GRU updates, while LeapVO [8] increases robustness in dynamic scenes via keypoints. While being great at optimizing the rotations via bundle adjustment, these methods fail to estimate the scale of the scene, making their applicability in real-world scenarios limited. Moreover, they require camera parameters and are slow, which makes their deployment difficult. In contrast, VoT directly regresses relative camera poses in metric space and does not require camera parameters.

Prior work introduced TSFormer [15], which predicts camera poses directly from video sequences using an end-to-end approach. However, its performance remains significantly below that of hand-crafted methods [8, 30] due to architecture, small training dataset, rotation representation, and inference scheme. Existing end-to-end methods struggle to perform in real-world settings because they rely on small, hard-to-scale architectures, and the gap between

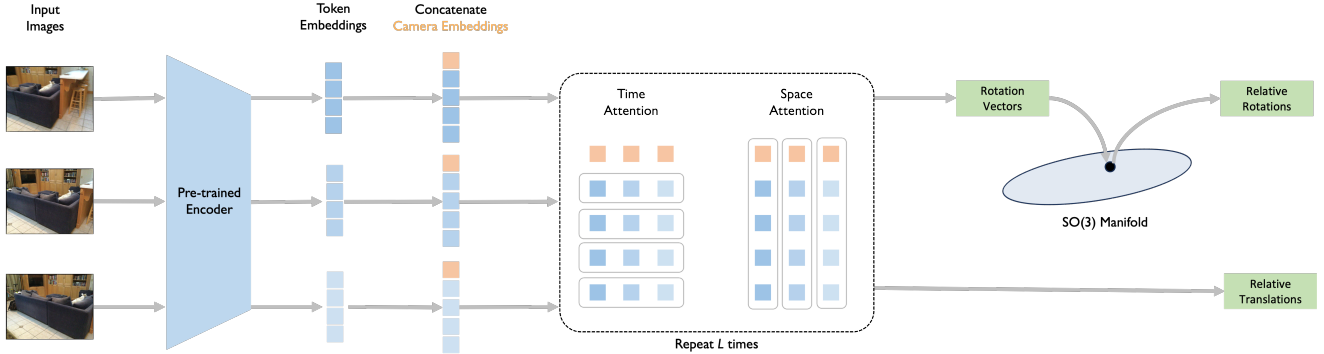


Figure 2. **VoT architecture.** Given multiple input frames, a frozen image encoder extracts per-image token embeddings. Camera embeddings are then concatenated to aggregate the information for camera pose estimation. The embeddings are decoded by L repeating decoder blocks with temporal and spatial attention modules. The rotations are projected onto the $SO(3)$ manifold to ensure valid relative rotations.

them and traditional methods remains substantial. By comparison, VoT uses a scalable end-to-end design which provided enough data to outperform traditional methods. When the data is limited, our method significantly reduces the performance gap between end-to-end and optimization-based pipelines, while being significantly faster.

Video transformers. Since their introduction in machine translation [32], transformers have become the dominant architecture in NLP [10, 23] and vision [17, 24]. Central to this framework, self-attention aggregates information across entire sequences, but its quadratic complexity makes direct application to videos inefficient. To mitigate this, prior work has proposed factorizing 3D attention into spatial and temporal components [45] or employing efficient variants such as divided space-time, sparse local-global, and axial attention [1, 3, 46]. In this work, we adopt the principle of efficient video learning by decoupling self-attention into separate temporal and spatial attention components.

Large 3D models. A trend in 3D vision is the development of large-scale models that jointly estimate camera poses and dense geometry [34–36], or learn versatile representations for downstream tasks [18, 39]. These models are increasingly viewed as foundational, yet despite strong task-agnostic results they suffer from drift on long video sequences and produce scale-ambiguous poses. In contrast, VoT focuses solely on the task of camera pose estimation, showing improved accuracy and less drift. Moreover, our model is significantly faster due to its size.

3. Method

In this section, we describe the architecture of VoT; see Fig. 2 for its overview. It consists of three main components: a pre-trained encoder to extract a compact representation of each frame, a transformer-based decoder, and a small feed-forward network that makes the final pose predictions. Unlike previous methods such as DVPO [30] or

LeapVO [8], VoT can be implemented in any deep learning framework, thanks to its streamlined architecture. Following the spirit of end-to-end frameworks [7], our inference code can be written purely in PyTorch, without additional complexities. We believe that the simplicity and accessibility of our approach will encourage further participation from the research community.

3.1. Architecture

Pre-trained encoder. We utilize pre-trained networks commonly employed in previous studies [36, 39] for encoding and extracting features from video frames. As the Vision Transformer (ViT) [11] has become the dominant architecture in computer vision, our pre-trained encoders are based on ViT. Specifically, we denote the sequence of input video frames as $V \in \mathbb{R}^{T \times H \times W \times 3}$, where T is the number of frames in the video and H, W denote the resolution of each frame. Each input image is then tokenized into $(h \cdot w)$ non-overlapping patches with $h = \frac{H}{p}$, $w = \frac{W}{p}$ and p as patch size. These tokens are processed through a series of ViT layers, producing image features $F \in \mathbb{R}^{T \times (h \cdot w) \times d}$, where d is the hidden dimension of the ViT. The ViT layer follows the standard architecture, consisting of a multi-head self-attention module and a feed-forward network. Since the transformer architecture is permutation-invariant, we augment it with sinusoidal position encodings [32].

Time-space decoder. The decoder consists of a stack of L identical layers, each containing three sub-layers. The first sub-layer is a multi-head temporal attention module, followed by a multi-head spatial attention module, and the final sub-layer is a feed-forward network. Unlike standard transformer layers that only use self-attention, the interleaving of temporal and spatial attention within the decoder layers enables each feature in a single frame to efficiently capture long-range dependencies with other features. This ability to learn long-context information effectively is crucial

when processing a large number of frames. As we demonstrate in our experiments, using a larger number of frames is key to achieving accurate camera pose predictions. To summarize the information in each frame, we use camera embeddings, which are learnable embeddings in spatial attention sub-layers.

We start by concatenating a camera embedding to each of the image features, resulting in input features to the decoder $F_0 = [\text{ce}, F] \in \mathbb{R}^{T \times (h \cdot w + 1) \times d}$ where $\text{ce} \in \mathbb{R}^{T \times 1 \times d}$ indicate the camera embeddings. We denote the inputs to the $(n + 1)$ th decoder layer by $F_n \in \mathbb{R}^{T \times (h \cdot w + 1) \times d}$. The $(n + 1)$ th decoder layer then outputs $F_{n+1} \in \mathbb{R}^{T \times (h \cdot w + 1) \times d}$ of the same size. Specifically, the temporal attention performs the scaled dot-product attention in the i -th head along the temporal dimension as¹:

$$\begin{aligned} \hat{Q} &= \hat{K} = \hat{V} = F[:, 1:, :]^\top, \\ \hat{Q}, \hat{K}, \hat{V} &\in \mathbb{R}^{(h \cdot w) \times T \times d} \end{aligned} \quad (1)$$

$$\begin{aligned} \hat{\text{head}}_i &= \text{Attention}(\hat{Q}W_i^{\hat{Q}}, \hat{K}W_i^{\hat{K}}, \hat{V}W_i^{\hat{V}}), \\ \hat{\text{head}}_i &\in \mathbb{R}^{(h \cdot w) \times T \times d_h}, \end{aligned} \quad (2)$$

where $W_i^{\hat{Q}}, W_i^{\hat{K}}, W_i^{\hat{V}} \in \mathbb{R}^{d \times d_h}$ are the learned projection matrices for query, key, and value. Here, we omit the layer index by treating $F_n = F$.

Note that we omit the camera embedding during the temporal attention computation since attention computation over learnable camera embeddings is redundant. The multi-head temporal attention aggregates $\hat{\text{head}}_{\{1 \dots h\}}$ together and then concatenates the camera embedding.

$$\begin{aligned} \hat{F} &= \text{Concat}(\hat{\text{head}}_1, \dots, \hat{\text{head}}_h)^\top W^{\hat{O}}, \\ \hat{F} &\in \mathbb{R}^{T \times (h \cdot w) \times d} \end{aligned} \quad (3)$$

$$\begin{aligned} \text{TemporalAttention}(\hat{Q}, \hat{K}, \hat{V}) &= [F[:, :1, :], \hat{F}], \\ \text{TemporalAttention} &\in \mathbb{R}^{T \times (h \cdot w + 1) \times d} \end{aligned} \quad (4)$$

where $W_i^{\hat{O}} \in \mathbb{R}^{d_h \times d}$ is the output projection and $F[:, :1, :]$ $\in \mathbb{R}^{T \times 1 \times d}$ indicates the camera embeddings copied from F .

Following the temporal attention, we apply the spatial attention along the spatial dimension, including the camera embedding as:

$$\bar{Q} = \bar{K} = \bar{V} = \hat{F} \in \mathbb{R}^{T \times (h \cdot w + 1) \times d_h} \quad (5)$$

$$\begin{aligned} \bar{\text{head}}_i &= \text{Attention}(\bar{Q}W_i^{\bar{Q}}, \bar{K}W_i^{\bar{K}}, \bar{V}W_i^{\bar{V}}) \\ &\in \mathbb{R}^{T \times (h \cdot w + 1) \times d_h}, \end{aligned} \quad (6)$$

¹The notation $[:, 1, :]$ indicates the submatrix that removes the first column, as in Numpy.



Figure 3. **Attention maps from the VoT decoder.** Each row shows an original image with a selected query (red square), followed by attention maps from the four subsequent frames. To estimate relative camera pose, VoT attends to the related image regions, resembling the behavior of classical keypoint-based odometry methods.

where $W_i^{\bar{Q}}, W_i^{\bar{K}}, W_i^{\bar{V}} \in \mathbb{R}^{d_h \times d_h}$ are the learned projection matrices for query, key, and value.

Similarly, the multi-head spatial attention aggregates $\bar{\text{head}}_{\{1 \dots h\}}$ together.

$$\begin{aligned} \text{SpatialAttention}(\bar{Q}, \bar{K}, \bar{V}) &= \text{Concat}(\bar{\text{head}}_1, \dots, \bar{\text{head}}_h)W^{\bar{O}} \\ &\in \mathbb{R}^{T \times (h \cdot w + 1) \times d} \end{aligned} \quad (7)$$

where $W_i^{\bar{O}} \in \mathbb{R}^{d_h \times d}$ is the output projection.

Ultimately, the camera embedding, $e \in \mathbb{R}^{T \times d}$, will be utilized to predict the camera poses for each frame.

3.2. Camera Poses Prediction

To regress the relative camera poses, the regression head takes a camera embedding from each frame as its input. A single linear layer then projects the embeddings to the rotation $\mathbb{F}_R \in \mathbb{R}^{(T-1) \times 9}$ and translation $\mathbb{F}_t \in \mathbb{R}^{(T-1) \times 3}$ vectors. Rotation vectors are projected to the closest valid rotation matrix by solving the special orthogonal Procrustes [4] problem:

$$\text{Procrustes}(\mathbb{F}_R) = \arg \min_{\hat{\mathbb{R}} \in SO(3)} \|\hat{\mathbb{R}} - \mathbb{F}_R\|_F^2.$$

The optimization problem is solved via singular value decomposition of \mathbb{F}_R following [31]. $\mathbb{F}_t \in \mathbb{R}^{(T-1) \times 3}$ is used as a translation prediction directly.

Decoding losses. The rotation loss, denoted as $\mathcal{L}_{\text{rotation}}(R, \hat{R})$, is the geodesic loss between the predicted rotation \hat{R} and the ground-truth rotation R , defined as

$$\mathcal{L}_{\text{rotation}}(R, \hat{R}) = \cos^{-1} \left(\frac{\text{Tr}(R^\top \hat{R}) - 1}{2} \right), \quad (8)$$

and the translation loss, denoted as $\mathcal{L}_{\text{translation}}$, is the L1 loss between the predicted translation \hat{t} and the ground-truth translation t :

$$\mathcal{L}_{\text{translation}}(t, \hat{t}) = \|t - \hat{t}\|_1. \quad (9)$$

The final loss for VoT training is a weighted loss between the rotation and translation losses:

$$\mathcal{L} = \lambda \cdot \mathcal{L}_{\text{rotation}} + \gamma \cdot \mathcal{L}_{\text{translation}}. \quad (10)$$

4. Experiments

Datasets. Our primary training leverages ARKitScenes [2], a large-scale dataset, providing rich and diverse indoor scenes. We further incorporate ScanNet [9] to broaden indoor coverage and KITTI [16] to expose the model to outdoor pose distributions. Out-of-distribution performance is evaluated on TUM.RGBD [27] which is not included in the training set. *ARKitScenes* [2] is a large-scale indoor dataset collected with LiDAR-equipped mobile devices, comprising over 5,000 sequences from 1,661 environments and totaling more than 11 million frames, making it one of the most comprehensive resources for indoor 3D scene understanding. To complement it, *ScanNet* [9] provides over 2 million frames across 1,613 scenes. For outdoor settings, *KITTI* [16] offers RGB images and ground-truth poses collected with GPS and LIDAR. Finally, *TUM.RGBD* [27] features indoor recordings with motion-capture ground truth. The datasets exhibit variation in camera calibration, poses, image resolution, as well as real-world artifacts such as rolling shutter, motion blur, and lighting variation.

Metrics. We evaluate visual odometry using Absolute Translation Error (ATE) and Absolute Rotation Error (ARE) [8, 30]. ATE is the RMSE of translation between estimated and ground-truth trajectories, while ARE is the RMSE of angular orientation differences. In addition, we report Relative Translation Error (RTE) and Relative Rotation Error (RRE), which measure the drift in translation and rotation over unit trajectory segments. In the tables, results are coded **best** and second best.

A note on alignment. While it is common practice to report evaluation metrics after applying rigid alignment and scale correction to the predicted trajectory, we believe this practice can be impractical for real-world applications, where ground-truth is unavailable. To take this real-world constraint into account we report both aligned and unaligned metrics.

Baselines. We compare our method against state-of-the-art visual odometry models [8, 30]. For DPVO [30], results are averaged over three runs with different random seeds to account for variability. We further benchmark against recent large-scale 3D models that directly predict camera poses [34, 35]. Because these models cannot process long video sequences in a single pass, inputs are split into temporally continuous chunks, with maximum lengths of 30 and 90 frames on our GPUs, respectively; the predicted poses are then concatenated to form the full trajectory. We also compare with a classical [6] and a state-of-the-art [21]

monocular SLAM systems, both using only RGB input. For fairness, loop closure is disabled during evaluation. Finally, we include a recent end-to-end visual odometry model [15] in our comparisons.

Implementation details. We use a frozen CroCo [41] backbone trained within the DUST3R [39] framework, consisting of 300 million parameters. We employ 12 alternating time-space attention blocks, totalling 200 million parameters, for the decoder. Our model is trained with the AdamW [20] optimizer for 300 epochs. We adopt a cosine learning rate schedule with an initial learning rate of 0.00001 and a warmup phase of 30 epochs. Our model takes 8 input views, sampled at intervals of 3 frames. Input frames are resized to a resolution of 224×224. Training runs on 12 NVIDIA RTX H100 GPUs for 5 days.

4.1. Visual Odometry Results

VoT is competitive without bells and whistles. As shown in Tabs. 1 to 3, VoT achieves competitive performance on both indoor and outdoor datasets, despite not relying on hand-crafted components. This is particularly notable in

Method	ATE [m] ↓	ARE [deg] ↓	RTE [m] ↓	RRE [deg] ↓
Aligned to GT				
ORB-SLAM3 [6] ^{†*}	1.08	133.92	0.03	4.01
DPVO [30] ^{†*}	0.49	<u>20.01</u>	<u>0.02</u>	<u>0.49</u>
LeapVO [8] ^{†*}	0.89	58.42	0.04	1.10
TSFormer [15]	141.34	56.32	0.37	0.62
CUT3R [34]	0.67	82.61	0.09	4.86
VGGT [35]	2.26	124.64	0.16	4.81
Mast3r-SLAM-VO [21]	<u>0.28</u>	25.49	0.19	17.89
VoT (Ours)	0.25	10.89	0.01	0.44
Unaligned to GT				
ORB-SLAM3 [6] ^{†*}	2.58	111.58	0.17	4.01
DPVO [30] ^{†*}	5.48	18.68	<u>0.04</u>	<u>0.48</u>
LeapVO [8] ^{†*}	28.31	49.25	0.62	1.09
TSFormer [15]	285.22	97.53	0.52	0.62
CUT3R [34]	2.42	97.70	0.12	4.86
VGGT [35]	2.94	92.37	0.15	4.81
Mast3r-SLAM-VO [21]	<u>0.60</u>	<u>14.40</u>	0.36	17.90
VoT (Ours)	0.51	13.40	0.01	0.44

Table 1. **Pose estimation metrics on ARKitScenes indoor settings.** Methods marked with [†] use bundle adjustment and methods marked with * use camera parameters. Provided enough training data, VoT shows superior performance.

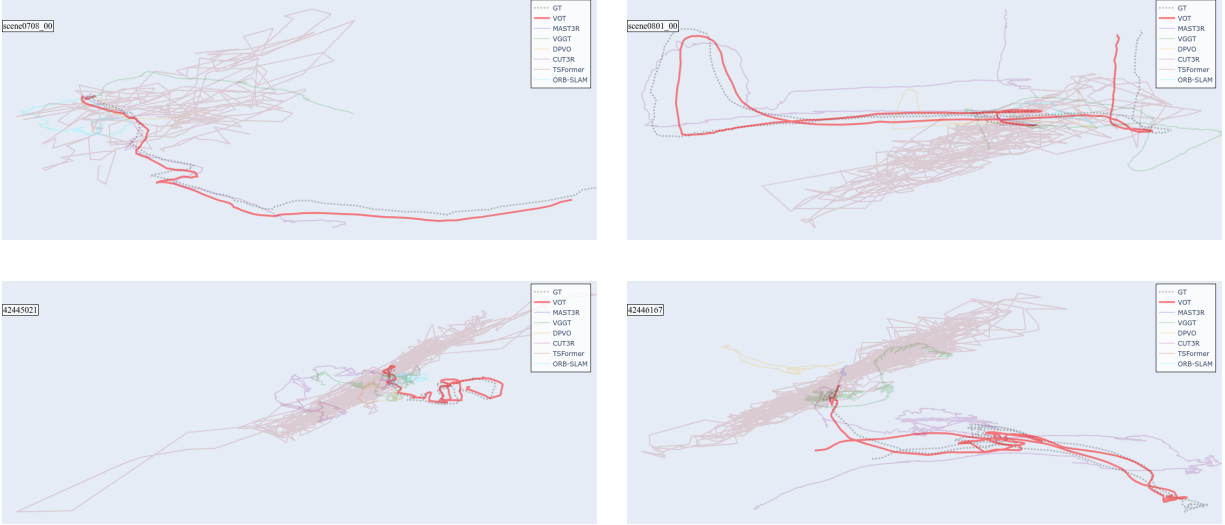


Figure 4. **Visualized Predicted Trajectories from Test Splits of ScanNet and ARKit Datasets.** Most methods cannot predict a coherent trajectory without aligning to the ground truth. In contrast, VoT predicts an accurate trajectory without alignment.

real-world settings, where *unaligned trajectory* metrics are more realistic due to the lack of ground-truth poses.

Large 3D models such as CUT3R [34] and VGGT [35], although trained on diverse multi-task 3D datasets - including both ScanNet and ARKitScenes - fail to generalize effectively. CUT3R and VGGT exhibit substantial drift in long sequences, while Mast3r-SLAM-VO [21] suffers from scale ambiguity and sparse predictions, resulting in degraded ATE and failure on the KITTI dataset.

Among odometry-specific methods, VoT exhibits strong generalization across datasets. In contrast, LeapVO [8], trained solely on synthetic data, struggles on real-world videos. DPVO [30] achieves competitive results on ScanNet and KITTI but fails to accurately estimate the scale (ATE). ORB-SLAM3 [6] fails to reliably estimate scale, leading to poor performance even with loop closure and bundle adjustment enabled. TSFormer [15], trained on a small dataset, without strong encoders or robust rotation representations, fails to predict accurate trajectories.

4.2. Ablation Studies

We conduct ablation studies to assess key design choices and analyze scaling trends with respect to model capacity and dataset size. For architectural ablations (e.g., attention mechanisms, backbone, and rotation representation), we use two input views with a stride of 10 and train for 150 epochs. For scaling experiments (e.g., varying dataset size), models are trained to convergence for 300 epochs to reflect scalability accurately. All ablations are evaluated on the ScanNet [9] dataset.

VoT delivers real-time prediction. To compare the speed between approaches, we measure their runtime on Scan-

Method	ATE [m] ↓	ARE [deg] ↓	RTE [m] ↓	RRE [deg] ↓
Aligned to GT				
ORB-SLAM3 [6] ^{†*}	1.07	141.78	0.04	3.75
DPVO [30] ^{†*}	<u>0.16</u>	<u>8.58</u>	<u>0.02</u>	0.34
LeapVO [8] ^{†*}	0.74	72.78	0.02	0.43
TSFormer [15]	105.21	61.42	0.32	0.45
CUT3R [34]	0.38	24.13	0.02	0.65
VGGT [35]	1.08	80.84	0.07	1.42
Mast3r-SLAM-VO [21]	0.22	19.31	0.22	6.59
VoT (Ours)	0.15	8.50	0.01	<u>0.42</u>
Unaligned to GT				
ORB-SLAM3 [6] ^{†*}	1.91	100.42	0.04	3.75
DPVO [30] ^{†*}	1.75	5.91	<u>0.02</u>	0.34
LeapVO [8] ^{†*}	10.84	43.60	0.09	0.43
TSFormer [15]	285.22	97.53	0.52	0.62
CUT3R [34]	4.85	135.52	0.02	0.65
VGGT [35]	1.56	31.73	0.06	1.42
Mast3r-SLAM-VO [21]	<u>0.99</u>	8.40	0.58	6.96
VoT (Ours)	0.34	<u>8.35</u>	0.01	<u>0.42</u>

Table 2. **Pose estimation metrics on ScanNet indoor settings.** Methods marked with [†] use bundle adjustment and methods marked with * use camera parameters. Without bells and whistles, VoT shows competitive performance.

Method	ATE [m] ↓	ARE [deg] ↓	RTE [m] ↓	RRE [deg] ↓
Aligned to GT				
ORB-SLAM3 [6] ^{†*}	80.81	157.31	2.82	1.29
DPVO [30] ^{†*}	<u>9.74</u>	13.63	<u>0.93</u>	0.06
LeapVO [8] ^{†*}	48.86	67.98	0.39	0.96
TSFormer [15]	15.77	93.57	0.45	0.74
CUT3R [34]	17.92	73.76	0.50	0.58
VGGT [35]	45.07	98.23	1.78	0.51
Mast3r-SLAM-VO [21]	X	X	X	X
VoT (Ours)	9.66	<u>31.12</u>	0.32	<u>0.42</u>
Unaligned to GT				
ORB-SLAM3 [6] ^{†*}	217.06	51.23	1.05	1.29
DPVO [30] ^{†*}	194.55	0.94	<u>0.85</u>	0.06
LeapVO [8] ^{†*}	211.80	39.78	0.94	0.96
TSFormer [15]	<u>140.10</u>	28.45	0.78	0.74
CUT3R [34]	112.36	22.07	0.71	0.58
VGGT [35]	205.67	16.32	2.13	0.51
Mast3r-SLAM-VO [21]	X	X	X	X
VoT (Ours)	63.10	<u>11.69</u>	0.65	<u>0.42</u>

Table 3. **Pose estimation metrics on KITTI outdoor settings.** Methods marked with [†] use bundle adjustment and methods marked with * use camera parameters. **X** denotes the methods that failed on some of the sequences. Even though KITTI training data amounts to only several videos, VoT shows competitive performance.

Net [9] *scene0000_00* using the same environment. As shown in Fig. 1, VoT achieves a considerably faster runtime, more than 3× speedup, compared to existing methods. This efficiency stems from its compact, end-to-end architecture, in contrast to larger 3D models. Moreover, unlike LeapVO, DPVO, and Mast3R-SLAM-VO, VoT does not rely on additional processing steps or bundle adjustment, contributing to both its speed and strong performance.

VoT is competitive on unseen datasets and camera parameters. Tab. 4 illustrates how VoT performs on a dataset not seen during training. Moreover, the camera parameters of the dataset are drastically different from those in the training set. While DPVO leverages effective bundle-adjustment for superior performance, VoT demonstrates competitive results and robust generalization compared to other methods.

VoT exhibits robust scaling behavior. Fig. 5 illustrates how VoT scales with respect to training data size and model capacity. VoT shows consistent performance improvements

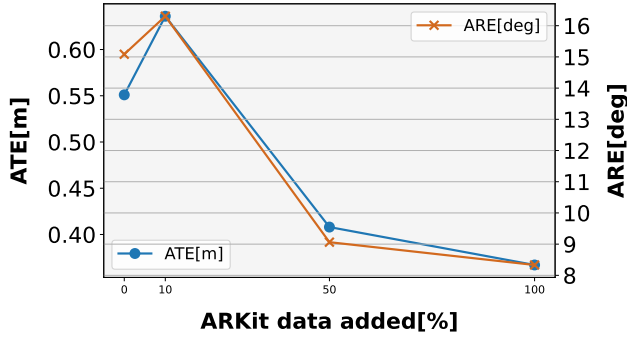
Method	ATE [m] ↓	ARE [deg] ↓	RTE [m] ↓	RRE [deg] ↓
Aligned to GT				
ORB-SLAM3 [6] ^{†*}	0.80	147.39	0.05	3.16
DPVO [30] ^{†*}	0.10	3.08	0.04	0.44
LeapVO [8] ^{†*}	X	X	X	X
TSFormer [15]	0.82	153.35	0.05	0.92
CUT3R [34]	0.87	29.42	<u>0.02</u>	1.41
VGGT [35]	1.05	70.34	0.03	0.77
Mast3r-SLAM-VO [21]	0.83	150.51	1.36	60.03
VoT (Ours)	<u>0.21</u>	<u>7.91</u>	0.01	<u>0.65</u>
Unaligned to GT				
ORB-SLAM3 [6] ^{†*}	1.65	76.14	0.03	3.16
DPVO [30] ^{†*}	<u>0.94</u>	3.01	0.07	0.44
LeapVO [8] ^{†*}	X	X	X	X
TSFormer [15]	200.87	105.86	0.58	0.92
CUT3R [34]	0.51	60.86	<u>0.02</u>	1.41
VGGT [35]	1.61	32.66	0.03	0.77
Mast3r-SLAM-VO [21]	1.21	47.81	1.32	60.03
VoT (Ours)	0.47	<u>10.37</u>	0.01	<u>0.65</u>

Table 4. **Pose estimation metrics on TUM_RGBD out-of-distribution setting.** Methods marked with [†] use bundle adjustment and methods marked with * use camera parameters. **X** denotes the methods that failed on some of the sequences. VoT performs well on unaligned metrics but lags behind in aligned settings.

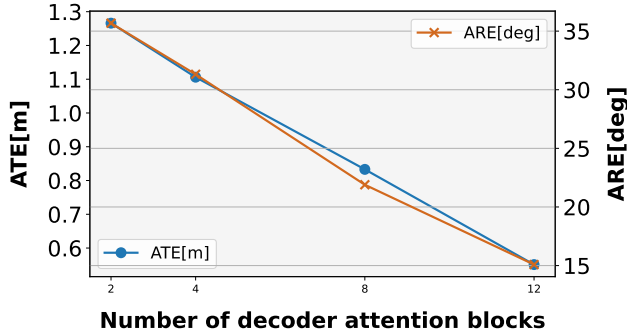
with both increased training data and a larger number of trainable parameters. Due to computational limits, we cap the number of decoder layers at 12. We analyze the scaling behavior with respect to encoder size and number of input views in the Supplementary Material.

Method	ATE [m] ↓	ARE [deg] ↓	RTE [m] ↓	RRE [deg] ↓
Euler Angles	0.78	20.64	0.05	1.47
Quaternion	0.68	18.92	0.05	<u>1.44</u>
Plucker Rays [44]	<u>0.66</u>	<u>16.11</u>	<u>0.05</u>	1.48
Rotation Matrix	0.55	15.09	0.04	1.25

Table 7. **Ablation of rotation representations.** Projecting predictions onto the nearest valid rotation matrix under the Frobenius norm yields the best performance.



(a) Scaling behavior w.r.t. training data



(b) Scaling behavior w.r.t. model capacity

Figure 5. **Scaling behavior of VoT.** As the model scales in (a) training data (proportion of ARKitScenes data added to ScanNet) and (b) model capacity (number of decoder layers), absolute translation and rotation errors decrease. This suggests that VoT exhibits robust scaling behavior.

Method	ATE [m] ↓	ARE [deg] ↓	RTE [m] ↓	RRE [deg] ↓
MAE	1.26	28.30	0.08	2.22
DinoV2	1.05	31.52	0.07	2.09
DinoV2*	0.96	<u>29.06</u>	0.07	<u>1.95</u>
CroCoV2	<u>1.02</u>	32.58	<u>0.07</u>	2.46
CroCoV2*	0.55	15.09	0.04	1.25

Table 5. **Backbone ablation.** CroCoV2* denotes the model trained within the Dust3r [39] framework, and DinoV2* denotes the backbone train in VGGT framework [35]. The results highlight the critical role of the architecture of the backbone, with geometry-focused supervision yielding better results across all metrics.

Architecture is the key determinant of backbone performance. We compare features extracted from various pre-trained backbones in Tab. 5. While DINOv2 [24] and CroCoV2 [41] yield comparable results, the CroCoV2 encoder trained within the Dust3R [39] framework that uses a geometry-focused architecture achieves substantially bet-

ter performance (i.e., approximately $2\times$ lower error across all metrics). Moreover, CroCoV2 trained within Dust3R framework shows superior performance to DinoV2 backbone trained on comparable amounts of data [35] and similar tasks. This suggests that the backbone architecture is the key components for a strong performance for our method.

SO(3) projection enhances rotation accuracy. In Tab. 7, we evaluate different rotation representations. Projecting outputs onto the nearest valid rotation matrix on the SO(3) manifold using the Frobenius norm consistently yields the best results, highlighting its suitability for our formulation.

Time-space attention achieves superior performance with lower computational cost. ?? compares full self-attention and time-space attention. Time-space attention not only reduces computational cost but also consistently improves accuracy. We attribute this to its matching-like spatial mechanism (see Fig. 3), where patches at corresponding locations across frames exchange temporal information, enhancing motion-aware feature encoding.

Limitations and future work. We do not claim VoT can generalize to all the datasets. Since it is trained on mostly static environments, performance may be limited in dynamic settings. Future improvements could come from scaling to more diverse datasets collected with different devices and careful calibration, as well as expanding coverage to a wider variety of scenes. Employing systematic data curation and incorporating larger models or advanced pre-trained components are also promising directions that could enhance both generalization and overall performance.

5. Conclusion

We presented VoT, an end-to-end method for visual odometry systems based on transformers for direct relative pose prediction. The approach achieves strong results compared to modern state-of-the-art odometry pipelines and large 3D models on the challenging indoor and outdoor datasets. VoT has a flexible architecture easily extensible to various backbones, with competitive results. Importantly, it can generalize to out-of-distribution camera parameters and image data. It exhibits strong scaling behavior, indicating that its performance could be further enhanced with sufficient data and computational resources. Finally, it is considerably faster than alternatives, being more compact than large 3D models, and, unlike other odometry systems, it does not require test-time optimization. We anticipate that future work will further advance end-to-end odometry systems.

Acknowledgements

This work has been financially supported by TomTom, the University of Amsterdam, and the allowance of Top consortia for Knowledge and Innovation (TKIs) from the Netherlands Ministry of Economic Affairs and Climate Policy.

References

- [1] Anurag Arnab, Mostafa Dehghani, Georg Heigold, Chen Sun, Mario Lučić, and Cordelia Schmid. Vivit: A video vision transformer. In *ICCV*, 2021. 3
- [2] Gilad Baruch, Zhuoyuan Chen, Afshin Dehghan, Tal Dimry, Yuri Feigin, Peter Fu, Thomas Gebauer, Brandon Joffe, Daniel Kurz, Arik Schwartz, and Elad Shulman. Arkitscenes: A diverse real-world dataset for 3d indoor scene understanding using mobile rgb-d data. In *NeurIPS*, 2021. 5
- [3] Gedas Bertasius, Heng Wang, and Lorenzo Torresani. Is space-time attention all you need for video understanding? In *ICML*, 2021. 3
- [4] Romain Brégier. Deep regression on manifolds: a 3D rotation case study. In *3DV*, 2021. 4
- [5] Cesar Cadena, Luca Carlone, Henry Carrillo, Yasir Latif, Davide Scaramuzza, Jose Neira, Ian Reid, and John J. Leonard. Past, present, and future of simultaneous localization and mapping: Toward the robust-perception age. *IEEE Transactions on Robotics*, 2016. 1, 2
- [6] Carlos Campos, Richard Elvira, Juan J. Gómez, José M. M. Montiel, and Juan D. Tardós. Orb-slam3: An accurate open-source library for visual, visual-inertial and multi-map slam. *IEEE Transactions on Robotics*, 2021. 2, 5, 6, 7
- [7] Nicolas Carion, Francisco Massa, Gabriel Synnaeve, Nicolas Usunier, Alexander Kirillov, and Sergey Zagoruyko. End-to-end object detection with transformers. In *ECCV*, 2020. 2, 3
- [8] Weirong Chen, Le Chen, Rui Wang, and Marc Pollefeys. Leap-vo: Long-term effective any point tracking for visual odometry. In *CVPR*, 2024. 2, 3, 5, 6, 7
- [9] Angela Dai, Angel X Chang, Manolis Savva, Maciej Halber, Thomas Funkhouser, and Matthias Nießner. Scannet: Richly-annotated 3d reconstructions of indoor scenes. In *CVPR*, 2017. 5, 6, 7, 1
- [10] Jacob Devlin, Ming-Wei Chang, Kenton Lee, and Kristina Toutanova. Bert: Pre-training of deep bidirectional transformers for language understanding. In *NAACL*, 2019. 3
- [11] Alexey Dosovitskiy, Lucas Beyer, Alexander Kolesnikov, Dirk Weissenborn, Xiaohua Zhai, Thomas Unterthiner, Mostafa Dehghani, Matthias Minderer, Georg Heigold, Sylvain Gelly, Jakob Uszkoreit, and Neil Houlsby. An image is worth 16x16 words: Transformers for image recognition at scale. In *ICLR*, 2021. 2, 3
- [12] Jakob Engel, Thomas Schöps, and Daniel Cremers. Lsdslam: Large-scale direct monocular slam. In *ECCV*, 2014. 1, 2
- [13] Jakob Engel, Vladlen Koltun, and Daniel Cremers. Direct sparse odometry. *TPAMI*, 2018. 2
- [14] Christian Forster, Luca Carlone, Frank Dellaert, and Davide Scaramuzza. Imu preintegration on manifold for efficient visual-inertial maximum-a-posteriori estimation. In *Robotics: Science and Systems*, 2015. 2
- [15] André O. Françani and Marcos R. O. A. Maximo. Transformer-based model for monocular visual odometry: A video understanding approach. *IEEE Access*, 2025. 2, 5, 6, 7
- [16] Andreas Geiger, Philip Lenz, and Raquel Urtasun. Are we ready for autonomous driving? the kitti vision benchmark suite. In *CVPR*, 2012. 5
- [17] Kaiming He, Xinlei Chen, Saining Xie, Yanghao Li, Piotr Dollár, and Ross Girshick. Masked autoencoders are scalable vision learners. In *CVPR*, 2022. 3
- [18] Vincent Leroy, Yohann Cabon, and Jerome Revaud. Grounding image matching in 3d with mast3r. In *ECCV*, 2024. 3
- [19] Shunkai Li, Xin Wang, Yingdian Cao, Fei Xue, Zike Yan, and Hongbin Zha. Self-supervised deep visual odometry with online adaptation. In *CVPR*, 2020. 2
- [20] Ilya Loshchilov and Frank Hutter. Decoupled weight decay regularization. In *ICLR*, 2019. 5
- [21] Riku Murai, Eric Dexheimer, and Andrew J. Davison. MAST3R-SLAM: Real-time dense SLAM with 3D reconstruction priors. In *CVPR*, 2025. 5, 6, 7
- [22] Duy-Kien Nguyen, Mahmoud Assran, Unnat Jain, Martin R. Oswald, Cees G. M. Snoek, and Xinlei Chen. An image is worth more than 16x16 patches: Exploring transformers on individual pixels. In *ICLR*, 2025. 2
- [23] OpenAI. Gpt-4 technical report. *arXiv preprint arXiv:2303.08774*, 2023. 3
- [24] Maxime Oquab, Timothée Darcet, Théo Moutakanni, Huy Vo, Marc Szafraniec, Vasil Khalidov, Pierre Fernandez, Daniel Haziza, Francisco Massa, Alaaeldin El-Nouby, Mahmoud Assran, Nicolas Ballas, Wojciech Galuba, Russell Howes, Po-Yao Huang, Shang-Wen Li, Ishan Misra, Michael Rabbat, Vasu Sharma, Gabriel Synnaeve, Hu Xu, Hervé Jegou, Julien Mairal, Patrick Labatut, Armand Joulin, and Piotr Bojanowski. Dinov2: Learning robust visual features without supervision. *TMLR*, 2024. 3, 8, 1
- [25] Anurag Ranjan, Varun Jampani, Lukas Balles, Kihwan Kim, Deqing Sun, Jonas Wulff, and Michael Black. Competitive collaboration: Joint unsupervised learning of depth, camera motion, optical flow and motion segmentation. In *CVPR*, 2019. 2
- [26] Alisha Sharma and Jonathan Ventura. Unsupervised learning of depth and ego-motion from cylindrical panoramic video. In *AIVR*, 2019. 2
- [27] J. Sturm, N. Engelhard, F. Endres, W. Burgard, and D. Cremers. A benchmark for the evaluation of rgb-d slam systems. In *IROS*, 2012. 5
- [28] Zachary Teed and Jia Deng. Deepv2d: Video to depth with differentiable structure from motion. In *ICLR*, 2020. 2
- [29] Zachary Teed and Jia Deng. Raft: Recurrent all-pairs field transforms for optical flow. In *ECCV*, 2020. 2
- [30] Zachary Teed, Lahav Lipson, and Jia Deng. Deep patch visual odometry. In *NeurIPS*, 2023. 2, 3, 5, 6, 7
- [31] S. Umeyama. Least-squares estimation of transformation parameters between two point patterns. *IEEE Transactions on Pattern Analysis and Machine Intelligence*, 1991. 4
- [32] Ashish Vaswani, Noam Shazeer, Niki Parmar, Jakob Uszkoreit, Llion Jones, Aidan N Gomez, Lukasz Kaiser, and Illia Polosukhin. Attention is all you need. In *NeurIPS*, 2017. 2, 3

- [33] Lukas Von Stumberg, Vladyslav Usenko, and Daniel Cremers. Direct sparse visual-inertial odometry using dynamic marginalization. In *ICRA*, 2018. [2](#)
- [34] Hengyi Wang and Lourdes Agapito. 3d reconstruction with spatial memory. In *3DV*, 2025. [3](#), [5](#), [6](#), [7](#)
- [35] Jianyuan Wang, Minghao Chen, Nikita Karaev, Andrea Vedaldi, Christian Rupprecht, and David Novotny. Vggg: Visual geometry grounded transformer. In *CVPR*, 2025. [5](#), [6](#), [7](#), [8](#)
- [36] Qianqian Wang, Yifei Zhang, Aleksander Holynski, Alexei A Efros, and Angjoo Kanazawa. Continuous 3d perception model with persistent state. In *CVPR*, 2025. [3](#)
- [37] Rui Wang, Martin Schwörer, and Daniel Cremers. Stereo dso: Large-scale direct sparse visual odometry with stereo cameras. In *ICCV*, 2017. [1](#), [2](#)
- [38] Sen Wang, Ronald Clark, Hongkai Wen, and Niki Trigoni. Deepvo: Towards end-to-end visual odometry with deep recurrent convolutional neural networks. In *ICRA*, 2017. [2](#)
- [39] Shuzhe Wang, Vincent Leroy, Yohann Cabon, Boris Chidlovskii, and Jerome Revaud. Dust3r: Geometric 3d vision made easy. In *CVPR*, 2024. [3](#), [5](#), [8](#)
- [40] Wenshan Wang, Yaoyu Hu, and Sebastian Scherer. Tartanvo: A generalizable learning-based vo. In *CoRL*, 2020. [2](#)
- [41] Philippe Weinzaepfel, Vincent Leroy, Thomas Lucas, Romain Brégier, Yohann Cabon, Vaibhav Arora, Leonid Antsfeld, Boris Chidlovskii, Gabriela Csurka, and Revaud Jérôme. Croco: Self-supervised pre-training for 3d vision tasks by cross-view completion. In *NeurIPS*, 2022. [5](#), [8](#), [1](#)
- [42] Zhichao Yin and Jianping Shi. Geonet: Unsupervised learning of dense depth, optical flow and camera pose. In *CVPR*, 2018. [2](#)
- [43] Vladimir Yugay, Theo Gevers, and Martin R. Oswald. Magic-slam: Multi-agent gaussian globally consistent slam. *arXiv preprint arXiv:2411.16785*, 2024. [2](#)
- [44] Jason Y Zhang, Amy Lin, Moneish Kumar, Tzu-Hsuan Yang, Deva Ramanan, and Shubham Tulsiani. Cameras as rays: Pose estimation via ray diffusion. In *ICLR*, 2024. [7](#)
- [45] Yanyi Zhang, Xinyu Li, Chunhui Liu, Bing Shuai, Yi Zhu, Biagio Brattoli, Hao Chen, Ivan Marsic, and Joseph Tighe. Vidtr: Video transformer without convolutions. In *ICCV*, 2021. [3](#)
- [46] Jiaojiao Zhao, Yanyi Zhang, Xinyu Li, Hao Chen, Shuai Bing, Mingze Xu, Chunhui Liu, Kaustav Kundu, Yuanjun Xiong, Davide Modolo, Ivan Marsic, Cees G.M. Snoek, and Joseph Tighe. Tuber: Tubelet transformer for video action detection. In *CVPR*, 2022. [3](#)

Visual Odometry with Transformers

Supplementary Material

6. Appendix

We test how well VoT scales with different backbone sizes and numbers of input views.

Performance of VoT with number of input views. Figure 6 illustrates how VoT, trained on the full dataset, scales with the number of input views. While the performance plateaus in terms of absolute metrics, it consistently improves in relative metrics. Due to computational constraints, the number of input views in our experiments is limited to a maximum of 12.

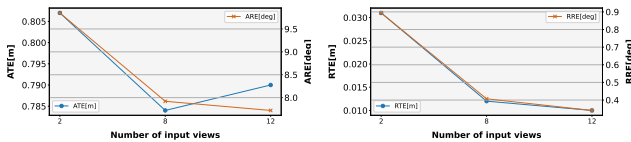


Figure 6. **Performance of VoT with number of input views on ScanNet [9] dataset.** As the number of input views increases, absolute translation and rotation errors initially decrease before plateauing. In contrast, relative metrics continue to improve steadily, highlighting the potential of VoT when using a long-range input sequence of views.

Performance of VoT with backbone size. In Fig. 7, we show how the performance of VoT varies with the size of the backbone. Since CroCO [41] is only available in a single size, we perform ablation using Dino-V2 [24] backbones. We observe that performance improves as the size of the backbone is increased. Due to computational limits, we cap the backbone size at DinoV2 [24] large.

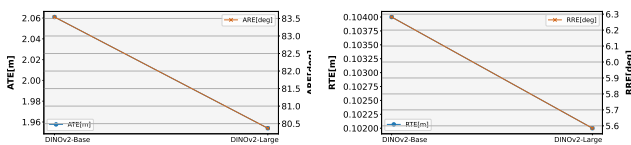


Figure 7. **Performance of VoT with backbone size on ScanNet [9] dataset.** As the number of backbone parameters increases, the model’s performance improves.